Journal of Molecular Structure: THEOCHEM 866 (2008) 34–45

Contents lists available at ScienceDirect

Journal of Molecular Structure: THEOCHEM

journal homepage: www.elsevier.com/locate/theochem

Theoretical study of the hexahydrated metal cations for the understanding of their template effects in the construction of layered double hydroxides

Hong Yan [a], Jun Lu [a], Min Wei [a,*], Jing Ma [b], Hui Li [b], Jing He [a], David G. Evans [a], Xue Duan [a]

[a] State Key Laboratory of Chemical Resource Engineering, Beijing University of Chemical Technology, The North Third Ring East Road 15#, Beijing 100029, PR China
[b] School of Chemistry and Chemical Engineering, Key Laboratory of Mesoscopic Chemistry of MOE, Nanjing University, Nanjing 210093, PR China

ARTICLE INFO

Article history:
Received 24 April 2008
Received in revised form 29 June 2008
Accepted 30 June 2008
Available online 11 July 2008

Keywords:
Hexahydrated metal ions
Layered double hydroxides
Template effect
Density functional calculation
Natural bond orbital
Structural direction

ABSTRACT

A series of octahedral hexahydrated metal cations as model formula $[M(OH_2)_6]^{n+}$ (M = metal cation, $n = 2$, 3 and 1 for M = Li) have been investigated by density functional theory (DFT) to shed light on their template effects in the construction for layered double hydroxides (LDHs) layers. The metal cations were classified to three types according to their calculated structural distortion angle θ as follows: Type I (canonical structure, θ: 0–1°), Type II (slightly distorted structure, θ: 1–10°) and Type III (heavily distorted structure, θ: >10°), respectively. The structure and properties of the hydrated cations such as bond distance, O–M–O bond angle distortion, binding energy, the valence electronic configuration, ligand field and Jahn–Teller effect and natural bond orbital (NBO), which are related to the construction of LDHs layers, were systematically investigated. It was found that in the case that the introduced cations which have close ionic radii to that of Mg^{2+}, the distortion angles of their octahedral hexahydrated metal cations (which are governed by the coordination environment of the metal ion) play more significant role of structure directing for the LDHs layers than the ion size. These cations can be introduced into LDHs layers with the availability in the following order: Type I > Type II > Type III. The coordination preference of the cations with much larger size in the formation of LDHs are also been discussed. The calculation-based rule is in good agreement with the experimental results.

1. Introduction

Layered double hydroxides (LDHs), also known as hydrotalcite-like materials and anionic clays, are available both as naturally occurring minerals and synthetic materials [1]. LDHs have brucite-like ($Mg(OH)_2$) intercalated structure and isomorphous replacement of trivalent cations for a fraction of divalent cations leads to the positively charged host layers, in which each metal cations M^{2+} or M^{3+} is coordinated by six oxygen atoms, forming the $M^{2+}/M^{3+}(OH)_6$ octahedron. These octahedra constitute the two-dimensional sheets via edge sharing, which then stack together by hydrogen bonding between the hydroxyl groups of adjacent sheets, balanced by a wide range of interlayer anions A^{n-} [2–4] (Fig. 1g), forming various kinds of LDHs materials represented by $[M^{2+}_{1-x}M^{3+}_x(OH)_2]^{x+}(A^{n-}{}_{x/n})\cdot mH_2O$ [2]. These layered solid materials have received considerable attention due to their potential applications in the fields of catalysis [1a], gene and molecular reservoir [1b], optical materials [1c], functional hybrid nanostructured materials [1d], controlled drug-release system [1e] and thin films [1f–h].

The above formula indicates that the value of the stoichiometric coefficient (x), the identities of the interlayer anions (A^{n-}) and the intra-layer cations can be varied over a wide range, which makes it possible to produce tailor-made materials for specific requirements. In recent years, many novel ternary and even quaternary LDHs have been synthesized [5]. In fact, the range of LDHs materials is even larger than suggested by the formula mentioned above because materials containing monovalent lithium ions of the type $[LiAl_2(OH)_6]^+[A^{n-}]_{1/n}\cdot yH_2O$ are also known and have similar structure [6].

Based on the previous abundant experimental work, an empirical rule for the LDHs synthesis has been drawn, i.e., a metal cation, which is incorporated into LDHs layers, should have an ionic radius not too different from that of Mg^{2+} (0.72 Å) [2]. Although it is very helpful for the LDHs construction, there are still some exceptions. For instance, according to this rule, many researchers attempted to introduce Pd^{2+} and Pt^{2+} with close ionic radii (0.86 and 0.80 Å, respectively) [7] to that of Mg^{2+} into LDHs layers due to their great potential application in catalysis. However, it has been reported that only trace of them can be introduced (0.04–5.0% atomic ratio percent) [8]. On the other hand, Ca^{2+} and Cd^{2+}, with much larger ionic radius (1.00 and 0.95 Å, respectively) than that of Mg^{2+}, have been reported to be incorporated into LDHs layers with a relatively large amount to form stable structure [9,10]. These results indicate that the ion size is not the only crucial factor that influences the construction of LDHs, as a result, it is necessary to find another criteria that can work together

---

* Corresponding author. Tel.: +86 10 64412131; fax: +86 10 64425385.
E-mail address: weimin@mail.buct.edu.cn (M. Wei).

0166-1280/$ - see front matter © 2008 Elsevier B.V. All rights reserved.
doi:10.1016/j.theochem.2008.06.031

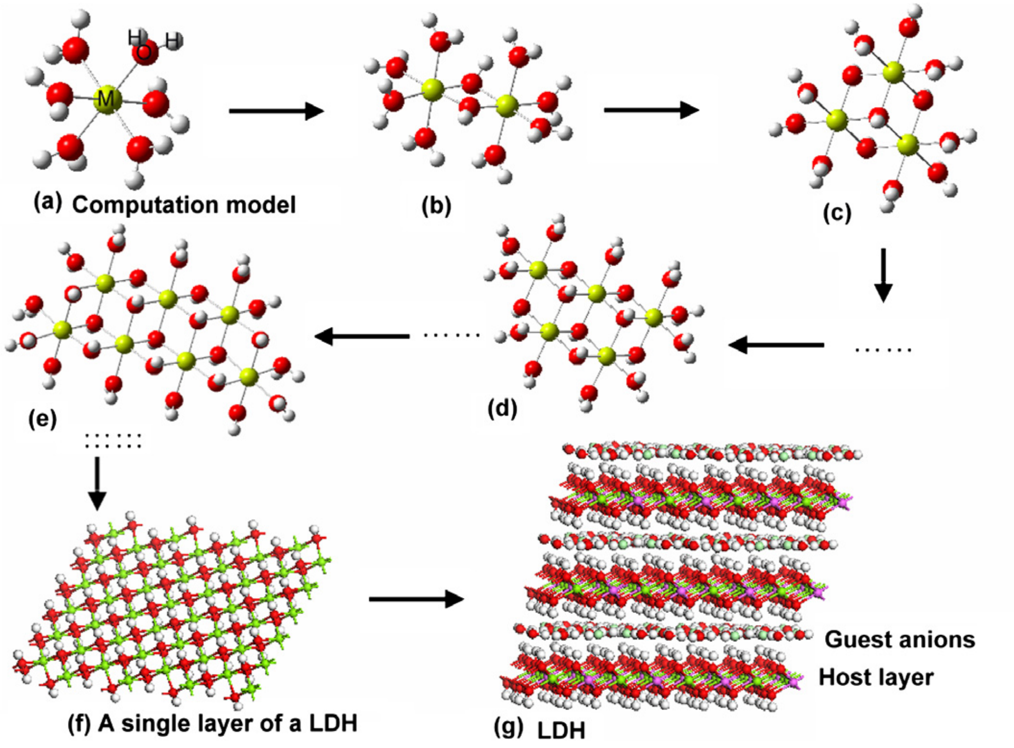

Fig. 1. Schematic representation of the initial template to form a LDH. (a) The calculation model $[M(OH_2)_6]^{n+}$ (M = metal cations, $n = 2, 3$) as the initial template; (b–e) top view of $[Mg_n(OH_2)_{n+6}(OH)_{2n-2}]^{2+}$ ($n = 2, 3, 5, 7$); (f) a single layer of a LDH; (g) a LDH consisting of brucite-like layers and guest anions.

with the ion size rule and then give more clear instruction for the design and preparation of LDHs materials.

It is well known that the method of coprecipitation is the most commonly used preparative technique for LDHs [3,4]. Recently, there has been an increasing interest in applications of LDH thin films to functional materials [1f–h]. Template-directed synthesis has been one of the most promising methods in the synthesis of inorganic films [11]. This method uses a floating monolayer as a template for the growth of a layered inorganic compound from an aqueous solution. Some efforts have been focused on clarifying such an effect from the viewpoint of structural consistency between a template and a growing crystal plane [12,13]. Herein, we attempt to extend this method to the formation of LDHs layer by theoretical study.

Recently, the use of computational methods for the study of LDHs has become an essential adjunct to experimental techniques for the analysis of the microstructure. Force-field based simulations (molecular dynamics and Monte Carlo methods) form the bulk of the literature on the modeling of LDHs systems to study the swelling properties, the arrangement of interlayer anions, the reactivity and other properties [1e,14]. However, such methods are unable to investigate the electronic structure inside LDHs layers, which is very important for the stability of the LDHs. Hence, quantum chemical calculations have been alternatively carried out. In general, for previous electronic structure studies of LDHs materials, two main models have been considered [15]: a semi-infinite model and a cluster model. The first one focuses on properties related with the whole bulk of the LDHs crystal in its whole extension by periodicity mainly with ab initio plane-wave density functional theory (PW-DFT) [16] or linear-combination of atomic orbitals (LCAO) methods [17]. The second one is used to cut a small piece of the solid (a cluster) including the main information for studying the property of LDHs. Semi-empirical molecular orbital method was employed [18a,b] to predict the geometry of layer structure, and the structural and chemical properties of the layers were also investigated by the density functional theory (DFT) [18c,d], claiming good agreement with experimental work. These studies show that the use of molecular cluster models is a valid approach for qualitative description of properties of LDHs layers. However, the cluster model were usually limited to a reasonable size that contains one or two kinds of cations in these studies (mostly Mg^{2+} and Al^{3+}) due to the demand for the computational cost.

In the present work, in order to study which cations can be introduced into the layers stably, we take a different insight into the formation of LDHs layer from the viewpoint of template effect. Since a LDH layer consists of edge-sharing octahedra of a mixture of di- and trivalent metal ions, it is reasonable for us to determine the most probable hexahydrated monomer of the metal ions $[M(OH_2)_6]^{n+}$ (M = metal cation) as the initial template to perform the density functional theoretic computation. By this way, we attempt to understand the template effect of the hexahydrated metal ions in the formation of the LDHs layer. Similar theoretical studies have been reported in the cases of Mg^{2+} in brucite [18c] and Al^{3+} in zeolite [19]. In this work, more di- and tri- valent hexahydrated metal ions which have been reported to be related to the LDHs layers (Table S3, Supplementary Information) are analyzed besides the most common hydrated Mg^{2+} and Al^{3+} ones. Moreover, the hydrated monovalent lithium ion is also investigated for the understanding of the formation of Li-Al-LDH.

According to the well-known crystal field theory and Jahn–Teller theorem, it can be expected that besides the ion size, the effects of the constrained environment of cations would also affect the relative stability of the octahedral hexahydrated metal ions. For instance, Cu^{2+} shows the Jahn–Teller effect significantly in the six-coordination environment, and for Pd^{2+} and Pt^{2+}, they prefer to be fourfold coordinated to form square-planar geometry. Although some studies have been focused on the coordination properties of metal cations sixfold coordinated to water [20], the template effect on the formation of LDHs layers are still unclear. Therefore, herein the characteristic coordination parameters (such as bond distance, bond angle and binding energy) of the octahedral hexahydrated metal ions are systematically discussed, and the valence electronic configuration of metal ions, Jahn–Teller effects and natural bond orbitals (NBO) which influence on the structure of octahedral hexahydrated metal ions have also been illustrated, so as to find out some rational rules other than the empirical ion size one for the preparation of prospective LDH compounds or related materials. The results provide important insight into formation of the main hydroxide layer, and quantitatively reveal that the distortion angle of the octahedral hexahydrated metal ions could be used as a more effective criterion for the construction of LDHs layers when an introduced cation has a close ionic radius to that of Mg^{2+}. It was found that the theoretical results are in high accordance with the experimental findings.

2. Computational method

2.1. Model of the octahedral hexahydrated metal ions as an initial template in the formation of LDHs layer

Since the metal–oxygen sixfold coordination octahedra are edge-shared in the LDHs layers, the edge length is an important factor for the formation of the LDHs layers. Consequently, in the formation of a layer, the O···O edge length of the initial template, octahedral metal ions, becomes an important factor for the formation of LDHs materials. It is evident that the metal ion included octahedron with closer O···O edge length to that of Mg^{2+} octahedron can combine with each other to form a layer more easily. As can be seen from Fig. 1a and b, the O···O edge length of octahedral metal ions is determined by both the M–O bond length and O–M–O angle, which actually indicates the two important factors related to the formation of LDHs layers. The former derives from the electrostatic interaction between metal ion and oxygen atom while the latter correlates to the coordination environment of the metal ion. However, the empirical criterion associated with the ionic size, which has been generally adopted in the LDHs construction, is only focused on the former factor. In contrast, the latter factor has received little attention before, although geometrically, the latter factor plays a more important role than the former due to the more significant contribution to the distortion of O···O edge length by the O–M–O angle than the M–O bond length. This is actually also the reason for the failure in explaining several LDHs formation (*vide supra*) on the basis of the empirical criterion. In this work, theoretical methods were used to understand the influence of O–M–O angle of the octahedral metal ions on the construction of the octahedral LDHs sheets. The model of the hexahydrated octahedral metal ion is shown in Fig. 1a with initial T_h symmetry [20].

To test the dependence of the template effect of the hexahydrated octahedral metal ions in the formation of LDHs layer, repeating calculations are extended to a system cluster contain a larger number of atoms modeled as formula $[Mg_n(OH_2)_{n+6}(OH)_{2n-2}]^{2+}$ ($n = 2$–7) consisting of 2–7 Mg atoms, since it includes only one kind of metal ion (Mg^{2+}), which greatly simplifies the identification of the crystal structure compared with other LDHs. In these models, each Mg–O–Mg bridging oxygen atom is set to be bonded to one hydrogen atom, and the terminal oxygen atoms are set to be bonded to two hydrogen atoms, in avoidance of the appearance of the unpaired electrons in the truncated ligands. Fig. 1b–e displays the top views of $[Mg_n(OH_2)_{n+6}(OH)_{2n-2}]^{2+}$ ($n = 2, 3, 5, 7$) clusters. The calculation results will be discussed in Section 3.1.

2.2. Density functional calculations

Theoretical calculations were carried out on the series of $[M(OH_2)_6]^{n+}$ (M = metal cation, $n = 2$, 3 and 1 for M = Li) cluster, where M is metal cation with di- and trivalence (Fig. 1a). For the transition periods, the ions are calculated only in high-spin state. Moreover, for some d^5 or d^6 ions such as Mn^{2+}, Ru^{3+}, Os^{3+}, Co^{3+}, Rh^{3+} and Ir^{3+}, which in most cases form low-spin ground-state complexes due to the larger ligand field stabilization energy (LFSE) in low-spin state configuration than in high-spin one [21], have also been calculated in low-spin state. At the same time, the models of $[Li(OH_2)_x]^+$ ($x = 2, 3, 4$) have been calculated for the comparison with their sixfold coordination complex.

The model geometrical optimization was performed by the density functional theory (DFT) with the three-parameter hybrid functional (B3LYP) [22]. The effective core potential (ECP), LANL2DZ [23], and the full electron basis sets, 6-31G(d) [24], were employed to the metal ions and OH_2 ligands, respectively. In addition, Mg, Ca, Al, Ga and Li have been treated with 6-31G(d) basis sets and CEP-121G basis set [25] were used for indium in order to test the performance of LANL2DZ basis sets. It was found that these two kinds of basis sets give comparable optimized geometries of $[M(OH_2)_6]^{n+}$ (M = Mg, Ca, Al, Ga and Li), as shown in Table 2.

The calculations were performed with the Gaussian 03 program suite [26]. No constraints were imposed on the geometry in any of the computations. The attainment of the energy minimum of each structure in full geometry optimization was tested by frequency calculations. The reported energies in this work were corrected by zero-point energy (ZPE).

2.3. Natural bond orbital analysis

Natural bond orbital (NBO) analysis has been demonstrated as a useful tool to provide chemists with a quantitative description of interatomic and intermolecular interactions in accordance with the classical Lewis structure concepts and with the basic Pauling–Slater–Coulson pictures of bond hybridization and polarization [27]. In the present work, we use NBO analysis to describe the bonding interaction between the metal ions and OH_2 ligands in the $[M(OH_2)_6]^{n+}$ model. The natural localized molecular orbitals/natural population analysis (NLMO/NPA) was also performed to illustrate the formation of the bond between them. We select different divalent cations which have been reported to be related to the LDHs layers and the trivalent cation Al^{3+} and Ga^{3+} which are the most commonly trivalent component in LDHs layers to perform the NBO calculations in high-spin state.

NBO analysis is carried out at the UB3LYP/LANL2DZ/6-31G(d) level using the NBO 5.0 program and built-in NBO 3.1 [28] subroutines of the Gaussian 03 program. The program NBOView 1.1 [29] is used for visualization of pre-NBO orbitals.

3. Results and discussion

3.1. The reliability to choose the model of the octahedral hexahydrated metal ions as an initial template in the formation of LDHs layer

A cluster model, $[Mg_n(OH_2)_{n+6}(OH)_{2n-2}]^{2+}$ ($n = 2$–7), is calculated for testify the reliability of our model for the octahedral hexahydrated metal ions $[M(OH_2)_6]^{n+}$ as an initial template in the formation of LDHs layer (Fig. 1). Suppose the formation of the cluster follows as the reaction as

$$2[Mg(OH_2)_6]^{2+} + 2OH^- \rightarrow [Mg_2(OH_2)_8(OH_2)]^{2+} + 4H_2O$$

$$[Mg_{n-1}(OH_2)_{n+5}(OH)_{2n-4}]^{2+} + [Mg(OH_2)_6]^{2+} + 2OH^- \rightarrow [Mg_n(OH_2)_{n+6}(OH)_{2n-2}]^{2+} + 5H_2O \quad (n = 3{-}7)$$

Table 1 summarizes binding energies and the optimized geometries of $[Mg_n(OH_2)_{n+6}(OH)_{2n-2}]^{2+}$ ($n = 2$–7) clusters. The binding energy is defined as:

Table 1
The comparison of the average interatomic distances and bond angles of the optimized geometries of $[Mg_n(H_2O)_{n+6}(OH)_{2n-2}]^{2+}$ (n = 2–7) clusters of the calculated and experimental results [30]

Number of Mg atoms	Average interatomic distance[b]/Å			Average angle[b]/degree		ΔE_{bind}/kcal mol^{-1}
	Mg–Mg	Mg–O	O···O	Mg–O–Mg	O–Mg–O	
1		2.101	2.969		89.91	347.28
2	3.082	2.029	2.629	98.84	80.75	1918.45
3	3.099	2.065	2.720	95.44	82.28	3469.56
4	3.101	2.062	2.727	96.22	82.50	5017.79
5	3.105	2.067	2.734	96.52	82.53	6565.63
6	3.109	2.061	2.728	95.91	82.09	8114.14
7	3.111	2.065	2.729	95.93	82.22	9839.78[c]
Exptl[a]	3.142	2.102	2.787	96.70	83.30	

[a] Experimental data of brucite crystal, Ref. [30].
[b] Only the edge-shared part is considered.
[c] Without ZPE correct.

$$\Delta E_{\text{bind}} = nE_{\text{Mg}^{2+}} + (n+6)E_{\text{H}_2\text{O}} + (2n-2)E_{\text{OH}^-} - E_{[\text{Mg}_n(\text{OH}_2)_{n+6}(\text{OH})^{2+}_{2n-2}]} \quad (n = 2\text{–}7) \tag{1}$$

where ΔE_{bind} denotes the total binding energy, which indicate the relative stability of the system, $E_{Mg}{}^{2+}$ denotes the calculated energy of the ground-state Mg^{2+}, E_{H_2O} = −76.4090 a.u., E_{H_2O}(ZPE) = −76.3878 a.u., E_{OH^-} = −75.1224 a.u. computed with 6-31G(d) basis set (1 a.u. = 627.51 kcal mol^{-1}), and $E_{[Mg_n(OH_2)_{n+6}(OH)_{2n-2}]^{2+}}$ denotes the total energy of the cluster, respectively. The binding energies listed in Table 1 were corrected by zero-point energy (the detailed results of each term in Eq. (1) are given in Supplementary Information Table S1).

Fig. 2a shows the dependence of the binding energy of a cluster on the size of a cluster. As is shown, the binding energy increases in proportion to the number of Mg atoms. It is, thus, expected that the larger the number of Mg atoms is, the more stabilized the oligomer is. On the other hand, the average distances of Mg–Mg, Mg–O and O···O edge decrease dramatically to minima as the Mg number varying from the one to two, and then increase to the value which are nearly constant (average 3.105, 2.064, 2.728 Å, respectively), as shown in Fig. 2b and Table 1. The average bond angle Mg–O–Mg and O–Mg–O follow the similar trend to those of the average distance (average constant value 96.00°, 82.32°, respectively). The calculated average constant interatomic distances and bond angles agree well with the experimental data for brucite (Table 1) [30]. This indicates that the hypothetical reaction of the formation of the layer is rational.

It is worth noting that for the average distances, there have slight deviation between the mono $[Mg(OH_2)_6]^{2+}$ cluster (2.102 Å) and the constant value (average 2.064 Å) when Mg atom number is larger than 2. However, for the average bond angle, the deviation is much larger (89.91° and 83.32°, respectively). This finding allows us to substantiate the earlier viewpoint that the O–M–O angle plays a more important role than the M–O bond length during the formation of the LDH layer. On the other hand, it also suggests that the O–M–O angle of the mono $[Mg(OH_2)_6]^{2+}$ cluster is the main factor influencing the formation of the LDH layer.

It can be expected that for the metal ion which has the close ion sizes to that of Mg^{2+}, if they show the close O–M–O angles, their O–M–O angle would distort in similar values and then easily to form a layer. Otherwise, the quite different distortion of the O–M–O angles would lead difficulty to form a layer. As a result, studying the electronic structure of different hexahydrated metal ion which related to the LDHs is helpful for the preparation of prospective LDHs compounds or related materials.

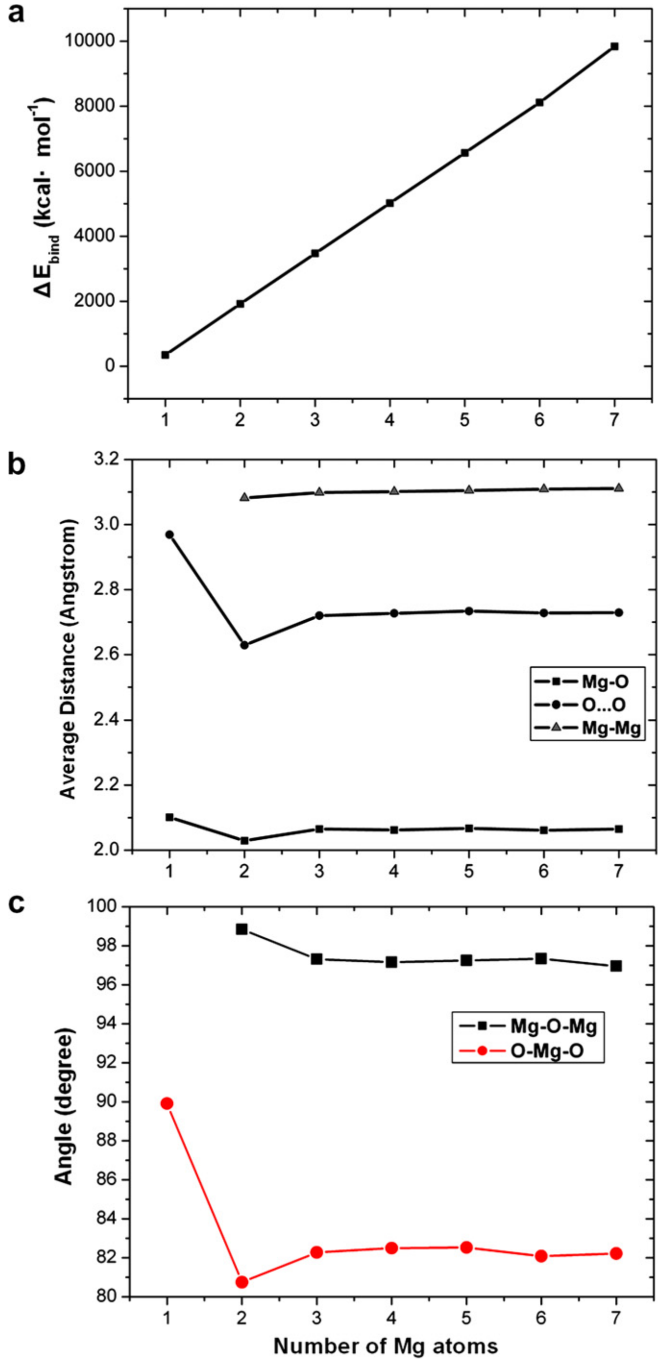

Fig. 2. (a) Binding energies (in kcal mol^{-1}), (b) average interatomic distances of Mg–Mg, Mg–O, O···O (in Å) and (c) bond angles Mg–O–Mg, O–Mg–O (in degree) of the optimized $[Mg_n(OH_2)_{n+6}(OH)_{2n-2}]^{2+}$ (n = 2–7) clusters as a function of the number of Mg atoms.

3.2. Classification of the calculated metal cations based on the distortion angles of octahedral hexahydrated metal ions

Through the geometric optimization at the DFT/(U)B3LYP level, the computation models show three different types of structure in the results (Fig. 3). The optimized structures are all shown with C1 symmetry. The geometry in Fig. 3a nearly has no distortion compared with the initial form, while Fig. 3b and c show a slight and a flatted heavy distortion, respectively.

As discussed above, the O–M–O angle in the octahedral hexahydrated metal ion is more crucial for the construction of LDHs

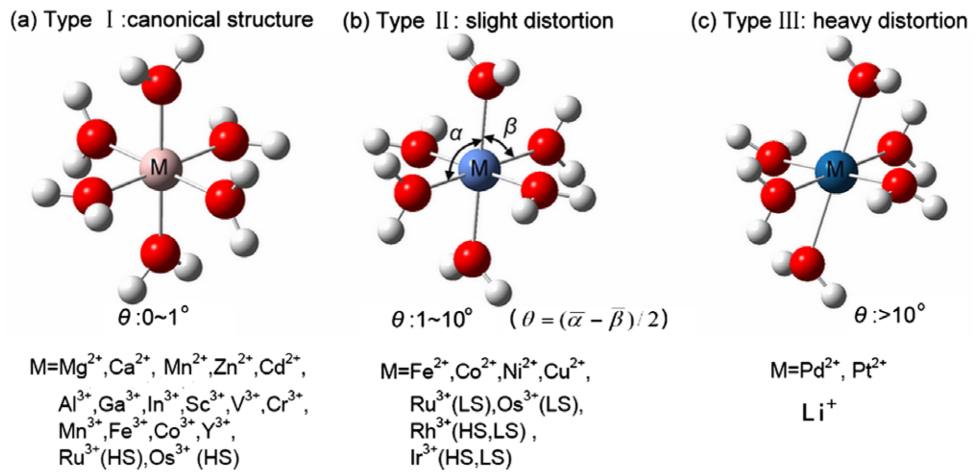

Fig. 3. Three types of optimized structures of the $[M(OH_2)_6]^{n+}$ (M = metal cation, n = 2, 3 and 1 for M = Li) models at (U)B3LYP/LANL2DZ/6-31G(d) level: (a) Type I (θ: 0–1°), (b) Type II (θ: 1–10°) and (c) Type III (θ > 10°).

layers. For the convenience to study the O–M–O angle, we defined the calculated structural distortion angle θ as:

$$\theta = (\bar{\alpha} - \bar{\beta})/2 \tag{2}$$

where $\bar{\alpha}$ and $\bar{\beta}$ denote the mean of the bond angle larger than 90° and smaller than 90°, respectively.

It can been seen from Fig. 3a that Mg^{2+} and Al^{3+} both have very small distortion angle (0.09° and 0.00°, respectively). Since Mg^{2+} and Al^{3+} are usually the main components of the LDHs layer, when another di- or trivalent metal ion is intend to be incorporated into the layer, it should combine with the Mg^{2+} or Al^{3+} to get the same O···O edge length to form an octahedral dimer at first based on the hypothetical reaction. Therefore, the distortion angle difference between each divalent ions and Mg^{2+} or between each trivalent ions and Al^{3+} can help us to analysis the corporation of these cations to the LDHs layers. Herein, we use the distortion angle directly to classify the calculated cations due to the zero-closed distortion angles of Mg^{2+} and Al^{3+}.

The geometries of the $[M(OH_2)_6]^{n+}$ models can be well characterized by their structural distortion angles. According to the values of distortion angle θ, the calculated ions can be classified into three categories as follows: (1) Type I: the canonical structure with θ in the range 0–1° (Fig. 3a); (2) Type II: slightly distorted structure with θ of 1–10° (Fig. 3b); (3) Type III: heavily distorted structure with θ larger than 10° (Fig. 3c). The metal cations of different types and their distortion angles are also listed in Table 2.

3.3. *Geometries and electronic configurations of the hydrated cations in different cation types*

The optimized metal–oxygen distances of three different types of ions compared with experimental values [31] are listed in Table 2. Some of the experimental values are estimated as the sum of the effective ionic radii given by reference [7] for cations in sixfold coordination and oxygen ions O^{2-} (1.40 Å). Recently, various metal hexahydrated ions have been investigated by means of quantum mechanical methods [20,32–34]. These calculations have reproduced experimental trends in metal–oxygen distances or hydration energies in a reasonable way. Some of the reported values are also listed in Table 2.

For Type I, the M–O bond lengths show the same value in different orientations except Cr^{2+} and Mn^{3+} which exhibit slightly elongated axial M–O distance. This is the result of Jahn–Teller effect, since in the crystal-field model where the overlap of metal and ligand orbital is neglected, the five metal d orbital split into a low-energy (t_{2g}) and a high-energy (e_g) set in the octahedral field. Cr^{2+} and Mn^{3+} ions have the same electronic configuration d^4 with an odd number of electrons in the two metal d orbital directed toward the ligands, d_{z^2} and $d_{x^2-y^2}$ [35].

In the case of Type II, the first transition metal $Cu^{2+}(d^9)$ ion shows strong Jahn–Teller effect with elongated axial M–O distance, while $Co^{2+}(d^7)$ and $Fe^{2+}(d^6)$ ions with compressed axial M–O distance. On the other hand, the low-spin Ru^{3+} and Os^{3+} (d^5) ions show weak Jahn–Teller effect with slightly elongated axial M–O distance, which is due to the uneven occupation of the degenerate t_{2g} orbital. In contrast to the ions in Type I, the stronger Jahn–Teller effect in Type II not only elongates or compresses the axial M–O distance, but also leads to heavier distortion of O–M–O bond angles. It should be noted that all the calculated low-spin ions are included in Type II. However, for some d^5 ions such as Mn^{2+}, Ru^{3+} and Os^{3+}, although they have larger distorted angles in their low-spin state classified to Type II, their high-spin state are included in Type I because of the less distorted angles.

Pd^{2+} and Pt^{2+} with d^8 configuration are the ions included in Type III. They have a triplet ground state with two electrons with parallel spins in the $e_g(O_h)$ orbital if being set in a weak octahedral field. However, if two axial ligands are removed from the system, giving a square-planar configuration of D_{4h} symmetry, the ligand field splits the e_g orbital into a pair with a_{1g} and b_{lg} symmetries [35]. For a strong D_{4h} ligand field this energy gain may be sufficient to stabilize square-planar low-spin geometry. This is the reason why these ions show much larger distorted angles than those of in Type I and Type II in an octahedral field.

On the other hand, the calculated M–O lengths of different types show some characters in common. The calculated bond lengths are close to the experimental mean distances (deviations ca. 0.1 Å) and in most cases longer than the experimental mean distances for the main group cations and the transition metal ions. It can be seen from Table 2 that for the transition metal ions, the M–O distances of the intermediate ions are shorter than expected, with minima for the d^3 and d^8 electronic configurations which have the largest ligand field stabilization energies. This trend is very similar to the change of ionic radii shown in the references [35]. As a result, the M–O distances change as follows for the same ion: divalence > trivalence; the M–O distances of high-spin ions are longer than those of low-spin ions for the transition metal ions.

In addition, the calculated ions in main groups (Mg^{2+} and Ca^{2+}) are included in Type I and they have the closed-shelled electronic configuration. Most of the calculated transition ions in Type I show the stable configuration such as s^0, d^0, d^5, d^{10} or d^2, d^3, d^4 in high-

Table 2

The classification of the calculated cations according to their calculated distortion angles of the $[M(OH_2)_6]^{n+}$, energy-optimized metal–oxygen distances and binding energies with zero-point energy(ZPE) correction, along with experimental or referred values

Cation	Spin	*R* (M–O)/Å		θ/degree	ΔE_{bind}/kcal mol^{-1}	
		Calcd	Exptl & Ref. [g]		Calcd	Ref.[t]
Type I						
$Mg^{2+}(3s^0)$	1	2.098 2.101[a]	2.102[h] 2.097[i,j]	0.09 0.05[a]	347.28[a]	282.80[u]
$Ca^{2+}(4s^0)$	1	2.428 2.424[a]	2.371[k] 2.400[l] 2.443[i,m]	0.20 0.02[a]	246.16 262.55[a] 282.22[a,r]	239.48 287.80[u]
Mn^{2+}(HS) $(3d^5)$	6	2.202	2.200–2.220[l]	0.41	326.74	327.20
$Zn^{2+}(3d^{10})$	1	2.132	2.080–2.100[l] 2.127, 2.142[i,n]	0.10	352.74	364.24 362.70[u]
$Cd^{2+}(4d^{10})$	1	2.312	2.350	0.31	308.12 323.00[r]	317.40
$Al^{3+}(3s^0)$	1	1.960 1.940[a]	1.907[i,h]	0.00 0.00[a]	730.47[a]	767.50[u]
$Ga^{3+}(4s^0)$	1	1.994 1.994[a]	2.020	0.03 0.15[a]	757.83[a]	722.04
$In^{3+}(5s^0)$	1	2.140 2.205[b]	2.200	0.00 0.06[b]	611.79[b]	602.77
$Sc^{3+}(3d^0)$	1	2.135	2.158[i,o]	0.05	606.97	576.24
$V^{3+}(3d^2)$	3	2.034	2.094[i,o]	0.74	696.91	638.86
$Cr^{3+}(3d^3)$	4	2.003	2.011[i,o]	0.12	725.14	671.13
$Mn^{3+}(3d^4)$	5	1.970[c] 2.160[d] 2.033[e]	2.038[i,o,e]	0.29	720.25	667.78
$Fe^{3+}(3d^5)$	6	2.052	2.050[i,o]	0.01	697.09	654.64
Co^{3+}(HS) $(3d^6)$	5	2.035	2.010	0.06	742.78	682.60
$Y^{3+}(3d^0)$	1	2.330	2.300	0.03	495.01	492.11
Ru^{3+}(HS) $(4d^5)$	6	2.247	2.080	0.04	600.96	555.21
Os^{3+}(HS) $(5d^5)$	6	2.283		0.04	592.60	
Type II						
Mn^{2+}(LS) $(3d^5)$	2	2.085[c] 2.016[d] 2.062[e]	2.070	3.63	386.54	
$Fe^{2+}(3d^6)$	4	2.162[c] 2.130[d] 2.151[e]	2.120[l]	1.06	348.70	342.97
$Co^{2+}(3d^7)$	4	2.123[c] 2.112[d] 2.119[e]	2.080–2.100[l]	3.78	369.35	353.01
$Ni^{2+}(3d^8)$	3	2.084	2.040–2.070[l]	4.49	378.30	368.07
$Cu^{2+}(3d^9)$	2	2.035[c] 2.271[d] 2.114[e]	2.300–2.400[q]	5.27	376.25	366.63
Co^{3+}(LS) $(3d^6)$	1	1.935	1.945	3.6	844.40	
Ru^{3+}(LS) $(4d^5)$	2	2.067[c] 2.130[d] 2.088[e]	2.014[q]	2.35	735.69	
Rh^{3+}(HS) $(4d^6)$	4	2.217	2.065	1.89	655.55	587.24
Rh^{3+}(LS) $(4d^6)$	1	2.077	2.016[q]	5.61	775.58	
Os^{3+}(LS) $(5d^5)$	2	2.078[c] 2.144[d] 2.100[e]		3.24	722.63	
Ir^{3+}(HS) $(5d^6)$	4	2.245	2.080	3.22	657.31	
Ir^{3+}(LS) $(5d^6)$	1	2.093		6.41	761.20	
Type III						
Pd^{2+} $(4d^8)$	3	2.269	2.260	10.29	412.08 68.68[s] 69.03[g]	329.59
$Pt^{2+}(5d)$	3	2.313	2.200	13.22	354.98 59.16[s] 72.22[g]	
$Li^{+}(1s^22s^0)$	1	2.171[f] 2.158[f] 2.165[e] 2.174[f,a] 2.16[f,a] 2.167[e,a] 1.953[g] 1.897[h] 1.861[r]	2.160 1.97[g,i,p] 1.92[h,i,p] 1.88[r,i,p]	14.55 14.97[a]	140.18 147.92[a] 24.65[s] 61.91[g] 51.76[h] 38.05[r]	

(*continued on next page*)

Table 2 (*continued*)

[a] All-electron 6-31G(d) basis sets.
[b] CEP-121 CEP basis sets.
[c] Equatorial length.
[d] Axial length.
[e] Average value.
[f] Different lengths along three orientations.
[g] Average value of fourfold coordination. Average binding energy = binding energy/coordination number, estimated as the sum of the effective ionic radii given by Ref. [7] for cations in sixfold coordination and oxygen ions O^{2-} (1.40 Å) if no superscript on the value.
[h] Average value of threefold coordination, Ref. [30a].
[i] Calculated value in the literature.
[j] Refs. [31a,32d].
[k] Ref. [31b].
[l] Refs. [31c] and [20b] and reference therein.
[m] Ref. [31d].
[n] Refs. [32g,32b].
[o] Ref. [34].
[p] Refs. [32f,33b].
[q] Ref. [20a] and references therein.
[r] Binding energy of sevenfold coordination, average value of twofold coordination.
[s] Average value of sixfold coordination.
[t] Estimated from Ref. [20a] without CAS correction if no superscript on the value.
[u] Ref. [31e].

spin state, while the ions in Type II are in transition period with d^6 or d^7 configuration in high-spin state and d^5 configuration in low-spin state, except the Ni^{2+} and Cu^{2+} ions with d^8 and d^9 configuration in the first transition period. However, the ions in Type III are not intended to form octahedral complexes. As a result, the high-spin state transition ions which have closed-shelled, half-filled configuration or have less electrons filled in e_g orbital show less angle distortion in geometry.

The only monovalent Li^+ ion with s^2 configuration is classified in Type III and shows two sets of M–O distance along three orientations. This is evidently not caused by Jahn–Teller effect, since the valence electrons are filled in s orbital without d splitting. The coordination between Li^+ and the ligands has no fixed orientation, as a result large distortions are found in $[Li(OH_2)_6]^+$ octahedral complex. Actually, the hydration number of Li^+ was 3–4, estimated from the chemical shift of proton NMR spectra [36], and the lithium ion usually has only four water molecules in the first coordination sphere according to the results of the previously reported calculation [33b].

As listed in Table 2, the calculated M–O distances are in accordance with the experimental [31] and calculation values in the literature [20,32–34] overall. Minor differences between our calculation results and the referred ones may be caused by the different experimental conditions and computational levels. For instance, the calculated geometries of $[Li(OH_2)_x]^+$ ($x = 2, 3, 4$) clusters in this work agree well with those in the literature [32f,33b], but the Li–O distances are slightly smaller than those reported in [33,33b]. This is due to different computational levels, i.e., MP2 and B3LYP level, which were used, respectively, in literatures and in this work. In the case of the trivalent ions of Sc, V, Cr, Mn and Fe, our calculation results also show minor differences from those of the literature [34], which is possibly caused by the different basis sets for metal ions used ((6-31+G*) in [34] and (LANL2DZ) in this work).

3.4. Binding energies of hydrated cations in different type

Binding energy of a system is usually used to be a criterion for the abilities of the metal ions combining with the ligands. The binding energy, which corresponds to a gas-phase reaction at 0 K, can be obtained based on the equation:

$$\Delta E_{\mathrm{bind}} = E_{\mathrm{M}^{n+}} + 6E_{\mathrm{H_2O}} - E_{[\mathrm{M(OH_2)_6}]^{n+}} \qquad (3)$$

where $E_{[\mathrm{M(OH_2)_6}]^{n+}}$ denotes the total energy of the $[M(OH_2)_6]^{n+}$ cluster and the denotation of the other symbols are the same as those of Eq. (1). The binding energies of the $[M(OH_2)_6]^{n+}$ ($n = 2, 3$) clusters given in Table 2 were corrected by zero-point energy (ZPE).

As shown in Table 2, the binding energies of all ions decrease with the increase of the ionic radii and M–O distance in general. For the same element, the divalent or high-spin state ion has lower binding energy than that of the trivalent or low-spin state ion. The lower binding energy of these ions is a result of the larger ion size. The overall binding energies of the 4d ions are lower than those of 3d ions while higher than those of 5d ions for the same electronic configuration in outer d shell, which is also related to the ion size.

The calculation results with two different basis sets for Mg^{2+}, Ca^{2+}, Al^{3+}, Ga^{3+} and In^{3+} are listed in Table 2. Slight deviation was found between the geometry parameters such as M–O bond length, bond angle distortion and binding energy calculated by LANL2DZ ECP basis sets and those calculated by all-electron 6-31G(d) basis sets or CEP-121G basis set (only for In^{3+}). However, the total energy calculated by all-electron 6-31G(d) basis sets or CEP-121G basis sets shows larger value than that of calculated by LANL2DZ ECP basis sets. Since the geometry and the binding energy are, in the present cases, not very sensitive to the change of the basis sets of the cations, we calculated all the other cations with LANL2DZ ECP basis sets in order to compute with the most efficient method yielding the necessary accuracy and make comparisons among cations at the same level.

It is to be noted that since Ru^{3+}, Os^{3+}, Rh^{3+} and Ir^{3+} ions have slightly lower zero-point energy corrected total energies in low-spin than those of in high-spin (see Table S2, Supplementary Information), it is evident that they have the low-spin grand-state, which is in agreement with the experiment results [21]. Consequently, both Ru^{3+} and Os^{3+} are classified into Type II. In contrast, Mn^{3+} and Co^{3+} are classified into Type I owing to their high-spin grand-state.

For the Pd^{2+} and Pt^{2+} ions in Type III, although their binding energies are not very low in an octahedral field, they would show larger binding energies to attain more stable low-spin square-planar structure [21]. The calculated average binding energies of fourfold Pd^{2+} and Pt^{2+} clusters $[M(OH_2)_4]^{2+}$ are listed in Table 2. They are larger than those of the sixfold ones, suggesting that they prefer to coordinate with OH_2 ligand in fourfold state to form square complexes.

Furthermore, since both experimental and theoretical studies of Ca^{2+} in solution indicate that 7, 8, and even 9 water molecules can be accommodated in the first solvation shell due to the large ionic radius of calcium [37], the calculation of the seven-water coordinated Ca^{2+} was performed. The same computation is carried out to Cd^{2+} owing to its large ion size. The calculated binding energies of sevenfold Ca^{2+} and Cd^{2+} clusters $[M(OH_2)_7]^{2+}$ listed in Table 2 are larger than those of the sixfold ones. This indicates that their more stable coordination preference is sevenfold other than six, though their sixfold coordination ions are also stable with little distortion angle.

It also can be seen from Table 2 that in the case of Li^+, all the calculated average binding energies (equal to binding energy divided by coordination number) of $[Li(OH_2)_x]^+$ ($x = 2, 3, 4$) clusters are larger than that of $[Li(OH_2)_6]^+$. The calculated average binding energy increases along with x changing from 2 to 4 (38.05, 51.76 and 61.91 kcal mol^{-1}, respectively), and then declines to a lower value of 24.65 kcal mol^{-1} when $x = 6$. This indicates that the Li–O bond is the most stable in the four-coordinated complex, and thus Li^+ prefers to form four- or threefold coordination complex other than sixfold one. This is consistent with the experimental results [36].

The calculated binding energies in Table 2 are in most cases larger than the calculation values in the literature, which may be caused by the different basis sets and different environments set to perform computation between our calculation and the literature work [20]. For instance, many reported data were obtained in solvent environment [20], while no constrains are imposed in our calculation.

3.5. Natural bond orbital analysis of the selected hexahydrated metal cations

For the understanding of the interaction between metal ion and OH_2 ligands in $[M(OH_2)_6]^{n+}$ ions, natural bond orbital (NBO) analysis was utilized in terms of a Lewis-like structure, and the $M–OH_2$ bonds are considered as donor–acceptor bonds [38]. Herein, we select the following divalent cations from different types: Mg^{2+}, Ca^{2+}, Zn^{2+}, Cd^{2+} (Type I); Fe^{2+}, Co^{2+}, Ni^{2+}, Cu^{2+} (Type II); Pd^{2+}, Pt^{2+} (Type III), which have been reported to be related to the formation of LDHs layers, to perform the NBO calculations. However, the same computations for trivalent cations are carried out only on Al^{3+} and Ga^{3+} (Type I), since they are the most common trivalent components of the LDHs.

The NBO analysis provides information about the Lewis and the non-Lewis (Rydberg) structure. Therefore, the electrons are located in bonds (BD) (electron pairs centered on two atoms), lone pairs (LP) (electron pairs centered on one atom), and core pairs (CR) (electron pairs centered on the core of one atom). The analyses of the individual electron densities were carried out separately for α (spin-up) and β (spin-down) orientations for the open-shelled systems. The latter reflect the two different opportunities by which a single electron can occupy a metal orbital in terms of the spin direction [27]. The percentage of the "natural lewis structure", NLMO/NPA bond orders between metal cation and oxygen atoms, the significant NBO interactions and their NBO stabilization energies $E(2)$ along the different orientations are listed in Table 3A. All the studied systems present more than 99% natural lewis structure, suggesting the dominance of the Lewis-type component of the bonding.

Firstly, let us focus the discussion on hexahydrated metal ions containing divalent cations. In general, the NBO representations of all systems studied show similar characteristics. The calculations of NBOs predict that they do not present a BD between the oxygen atoms and the divalent cations, i.e., no formal metal–oxygen bonding orbital is identified among the NBOs in each of these studied divalent octahedral hexahydrated metal ions. In contrast, as shown in Table 3A, the interaction between the metal atom and oxygen atom is seen through an electronic delocalization between bond orbitals from O hybrid orbitals containing s character and p character to metal pure $(n + 1)$s or d orbitals. The electronic delocalizations are estimated by second order perturbation theory from the stabilization energy $E(2)$ associated with the donor–acceptor interaction between two NBOs [28b]. For the divalent systems including Type I and Type II cations, the most significant interactions are delocalization from O sp hybrid orbitals to metal $(n + 1)$s orbitals. On the other hand, for the open-shelled hexahydrated metal ions consisting of Fe^{2+}, Co^{2+}, Ni^{2+} and Cu^{2+}, another second significant interaction takes place from O sp hybrid orbitals to metal d orbitals, since these metal ions have unoccupied d orbitals. Pre-NBOs (PNBOs), which are a set of localized Lewis NBO precursors that lack the final interatomic orthogonalization step, provide a convenient way to visualize interactions between orbitals in different bond regions, because their overlap is proportional to their interaction energy [39]. The 3D view and 2D contour of pre-NBOs for the most significant interactions of the calculated Type I and Type II divalent hexahydrated metal ions are illustrated on *xz* plane in Fig. 4a. It is shown that the σ-interaction from O sp hybrid orbitals to metal $(n + 1)$s orbitals are very strong in these systems. However, it is quite different for the Type III (Pd^{2+}, Pt^{2+}) systems. The most significant interactions are not the delocalization from O sp hybrid orbitals to metal $(n + 1)$s orbitals, but the delocalization from O sp^2 hybrid orbitals to metal d orbitals, as displayed in Fig. 4b. It can be seen from Fig. 4a and b that the overlap between O sp_x lone pair and Mg 3s orbital in $[Mg(OH_2)_6]^{2+}$ displays the same phase, but the overlap between O $sp^2{}_x$ lone pair and Pd $4d_{z^2} - 4d_{x^2-y^2}$ hybrid orbital in $[Pd\ (OH_2)_6]^{2+}$ shows the opposite phase, indicating the more stronger M–O interaction in $[Mg(OH_2)_6]^{2+}$.

The contributions of *n*d interaction and $(n{+}1)$s σ-interaction to charge transfer in $[M(OH_2)_6]^{n+}$ in electrons are reported in Table 3B. The amount of electron density shifted from the oxygen donor lone pairs (LPs) to the metal ions was judged by means of occupation numbers of the formally unoccupied *n*d and $(n{+}1)$s orbitals in the NBO basis for divalent cations. Applications of this method in the analysis of electronic structure of 3d $[M(H_2O)_6]^{3+}$ ions have been reported recently [34]. As can be seen in Table 3B, the total amount of charge transfer obtained in this way is virtually identical to the occupancy of *n*d and $(n{+}1)$s orbitals of natural electron configuration of the systems obtained via natural population analysis (NPA) of the natural atomic orbitals (NAOs) [27a]. The agreement between these numbers shows that delocalization of metal electrons into empty antibonding orbitals at the ligands and *n*p metal orbitals does not contribute significantly to the M–L interaction in these cases. In addition, the system including closed-shelled Type I cations (Mg^{2+}, Ca^{2+}, Zn^{2+}, Cd^{2+}) shows the strongest σ-interaction (>80%) and the weakest d interaction (<0.1%); the system including open-shelled Type II cations (Fe^{2+}, Co^{2+}, Ni^{2+}, Cu^{2+}) shows the moderate σ-interaction and *d* interaction (about 50%); Type III cations (Pd^{2+}, Pt^{2+}) contained system exhibits the weakest σ-interaction (<40%) and the strongest d interaction (>59%). From this point of view, the Type I cations reveal the strongest stability in hexahydrated metal ions, while the stability of the Type III cations are not significant, since the s orbital is sphere and the interaction between s orbital and O LPs are stronger than that of between d orbital and O LPs along three orientations. This is consistent with the result which has been obtained above.

The most common trivalent cation components in LDHs layers, Al^{3+} and Ga^{3+} (Type I), have also been demonstrated by the NBO analysis. As displayed in Table 3A and B and Fig. 4c, formal metal–oxygen bonding orbital exists in these studied systems, and the most significant interaction is the delocalization from the M–O σ-bonding orbital to the M–O σ-antibonding orbital. These interactions are very strong with larger stabilization energies $E(2)$ (17.89 and 21.56 kcal mol^{-1} for Al and Ga hexahydrated metal ions, respectively) than those of divalent systems except Mg^{2+} (26.22 kcal mol^{-1}). This further confirms the relative stability of

Table 3
Calculated NBO parameters of the selected $[M(OH_2)_6]^{n+}$ clusters at the B3LYP/LANL2DZ level of theory

(A) The percentage of the "natural lewis structure", NLMO/NPA bond orders between metal cation and oxygen atoms, the difference between the maximum and minimum of the bond orders ΔBO, and the significant NBO interactions and their NBO stabilization energies $E(2)$ by second order perturbation theory analyses

Cation	Spin	%Lewis	Orientation	NLMO/NPA		ΔBO [a]	The significant NBO interactions [b]		$E(2)$/kcal mol^{-1}
				M–O Orders	Bond		Donor LP(O)	Acceptor LP*(M)	
Type I									
Mg^{2+}		99.54	*x y z*	0.0430		0	$sp^{1.08}$	3s	26.22
Ca^{2+}		99.75	*x y z*	0.0281		0	$sp^{1.02}$	4s	11.43
Zn^{2+}		99.65	*x y z*	0.0191		0	$sp^{1.06}$	4s	9.51
Cd^{2+}		99.73	*x y z*	0.0178		0	$sp^{1.02}$	4s	6.59
Al^{3+}		99.45	*x y z*	0.1521		0	σ_{Al-O}	σ_{Al-O}^*	17.89
Ga^{3+}		99.36	*x y z*	0.1736		0	σ_{Ga-O}	σ_{Ga-O}^*	21.56
Type II									
Fe^{2+}	α	99.63	*z*	0.0145		0.0389	$sp^{1.05}$	4s	9.68
			x	0.0140					9.48
			y	0.0155					10.34
	β	99.09	*z*	0.0486			$sp_z^{1.01}$	4s	9.28
								$3d_{xz}+3d_{yz}+3d_{x^2-y^2}$	6.97
			x	0.0446			$s_{zx}^{1.01}$	4s	9.30
								$-3d_{xy}$	7.73
								$-3d_{xz}+3d_{yz}$	
			y	0.0529			$sp_y^{1.00}$	4s	11.50
								$3d_{xz}+3d_{yz}+3d_{x^2-y^2}$	4.70
Co^{2+}	α	99.63	*z x y*	0.0166		0.0343	$sp^{1.04}$	4s	10.86
	β	99.10	*z*	0.0509			$sp_z^{0.79}$	4s	10.75
								$3d_{xy}+3d_{xz}-3d_{x^2-y^2}$	5.43
			x	0.0476			$sp_x^{1.07}$	4s	10.97
								$3d_{xz}+3d_{yz}-3d_{x^2-y^2}$	6.56
			y	0.0453			$sp_y^{1.60}$	4s	11.25
								$3d_{xy}+3d_{xz}-3d_{x^2-y^2}$	4.69
Ni^{2+}	α	99.62	*z x*	0.0179		0.0362	$sp^{1.27}$	4s	11.72
			y	0.0168					
	β	99.03	*z y*	0.0530			$sp^{1.28}$	4s	12.96
								$-3d_{z^2}+3d_{x^2-y^2}$	5.68
			x	0.0494			$sp_x^{1.23}$	4s	11.23
								$3d_{x^2-y^2}$	8.70
Cu^{2+}	α	99.61	*z*	0.0145		0.0633	$sp_z^{1.13}$	4s	7.39
			x	0.0207			$sp_x^{1.50}$	4s	13.20
			y	0.0228			$sp_y^{1.60}$	4s	13.70
	β	99.09	*z*	0.0141			$sp_z^{1.12}$	4s	7.35
			x	0.0577			$sp_x^{1.69}$	4s	14.12
								$3d_{x^2-y^2}$	5.40
			y	0.0774			$sp_y^{1.84}$	4s	13.89
								$3d_{x^2-y^2}$	7.92
Type III									
Pd^{2+}	α	99.72	*z y*	0.0143		0.0798	$sp^{1.87}$	5s	6.94
			x	0.0134					
	β	98.77	*z*	0.0772			$sp_z^{2.23}$	$-4d_{z^2}-4d_{x^2-y^2}$	7.69
			x	0.0932			$sp_x^{2.23}$	$4d_{z^2}-4d_{x^2-y^2}$	12.09
				0.0944					
			y	0.0921			$sp_y^{2.37}$	$-4d_{z^2}-4d_{x^2-y^2}$	10.73
				0.0939					
Pt^{2+}	α	99.70	*z*	0.0199		0.0807	$sp^{2.18}$	6s	9.22
			x	0.0226					9.37
			y	0.0217					9.34
	β	99.02	*z*	0.0977	0.1006		$sp_z^{2.66}$	$5d_{z^2}-5d_{x^2-y^2}$	12.96
			x	0.0985	0.1005		$sp_x^{2.61}$	$-5d_{z^2}-5d_{x^2-y^2}$	15.06
			y	0.0874			$sp_y^{2.62}$	6s	10.38

(B) Natural charge of metal cations (q_M), charge transfer (Δq) of cations and contributions of *n*d interaction and (*n*+1)s σ-interaction to charge transfer in $[M(OH_2)_6]^{n+}$ in electrons

Type	Cation	Natural electron configuration	q_M	Δq[c]	$(n+1)s$[d]σ		*n*d[d]	
					Total	%Δ*q*	Total	%Δ*q*
I	Mg^{2+}	3s(0.25)3p(0.01)	1.728	0.272	0.251	92.27	0.000	0.00
	Ca^{2+}	4s(0.13)3d(0.01)5p(0.02)	1.839	0.161	0.131	81.36	0.000	0.00
	Zn^{2+}	4s(0.23)3d(9.99)4p(0.01)5p(0.01)	1.754	0.246	0.233	94.71	0.0014	0.57
	Cd^{2+}	5s(0.21)4d(9.99)5p(0.02)	1.768	0.232	0.210	90.51	0.0011	0.49
	Al^{3+}	3s(0.35)3p(0.57)3d(0.02)4p(0.01)	2.059	0.941				
	Ga^{3+}	4s(0.52)4p(0.54)4d(0.01)5p(0.01)	1.926	1.074				
II	Fe^{2+}	4s(0.21)3d(6.20)4p(0.02)4d(0.01)	1.563	0.436	0.214	49.08	0.220	50.46
	Co^{2+}	4s(0.23)3d(7.19)4p(0.02)	1.552	0.448	0.229	51.11	0.213	47.54
	Ni^{2+}	4s(0.24)3d(8.23)4p(0.02)	1.505	0.495	0.242	48.88	0.240	48.48
	Cu^{2+}	4s(0.26)3d(9.20)4p(0.02)	1.515	0.485	0.257	52.99	0.214	44.12
III	Pd^{2+}	5s(0.20)4d(8.45)5p(0.03)5d(0.01)	1.322	0.678	0.192	28.31	0.472	69.62
	Pt^{2+}	6s(0.31)5d(8.40)6p(0.03)6d(0.01)	1.249	0.751	0.294	39.14	0.445	59.25

[a] The difference between the maximum and minimum of the bond orders.

[b] The NBO stabilization energies $E(2)$ of back donations are below the threshold for printing (<0.25 kcal mol^{-1}) in NBO analysis.

[c] Total charge transfer obtained via NPA.

[d] Sum of occupation numbers of formally empty metal NBOs.

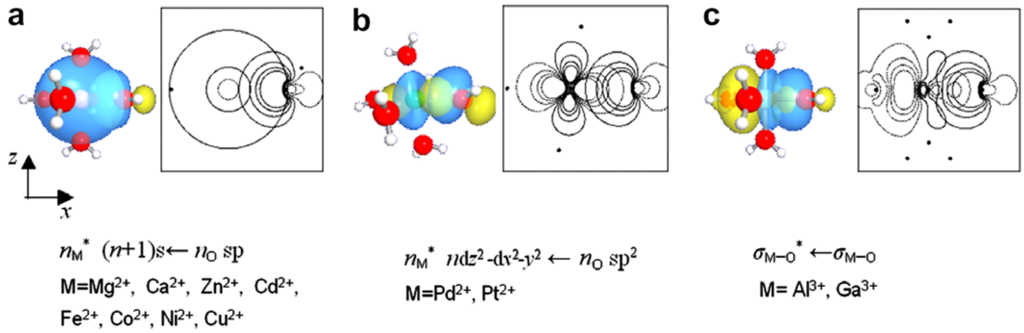

Fig. 4. The most significant NBO interactions of calculated $[M(OH_2)_6]^{n+}$ clusters represented by the overlap between: (a) the O sp$_x$ lone pair and the Mg 3s orbital in $[Mg(OH_2)_6]^{2+}$; (b) the O sp$^2{}_x$ lone pair and the Pd $4d_{z^2} - 4d_{x^2-y^2}$ hybrid orbital in $[Pd\ (OH_2)_6]^{2+}$; (c) the Al–O σ-bonding orbital and the Al–O σ-antibonding orbital in $[Al(OH_2)_6]^{3+}$. The 3D and 2D pre-orthogonalized NBOs were generated with the NBOView program.

octahedral hexahydrated metal ions containing Mg^{2+}, Al^{3+} and Ga^{3+}.

The natural localized molecular orbitals/natural population analysis (NLMO/NPA) bond orders [27] in Table 3A indicate the interaction of the M–L bonding. The bond orders are listed for three orientations(x, y and z) and two spin states (α and β). It is well known that the larger the bonder order is, the stronger the bond strength is. As shown in Table 3A, the systems including closed-shelled Type I cations represent the same bond order in different orientations, indicating the same strength of each M–L bond in different orientations. Moreover, trivalent cations Al^{3+} and Ga^{3+} have much larger bond orders (0.1521 and 0.1736, respectively) than those of divalent cations. This suggests that the octahedral hexahydrated metal ions consisting of these cations possess canonical geometries, which is in agreement with the previous calculations. It can be expected that distortion will occur if the bond strength of the different orientations shows different value. Therefore, the calculated systems including Type II and Type III cation exhibit different bond orders along different orientations, implying their distorted geometries. For the purpose of estimating of the distortion, the difference between the maximum and minimum of the M–L bond orders (ΔBO) of each system has been listed in Table 3A. The ΔBOs of the Type II cations are less than the Type III cation, which indicates that the distortions in hexahydrated metal ions including Type II are weaker than those in Type III. This accounts well for the above-mentioned trend in distortion angle: Type I < Type II < Type III. Furthermore, the Jahn–Teller effect of some ions was also suggested by the bond order analysis. The Cu^{2+}(d^9) ion shows strong Jahn–Teller effect with much longer axial M–O bond orders than the equatorial ones, which leads to the elongated axial M–O bond length. In contrast, Co^{2+}(d^7) and Fe^{2+}(d^6) ions exhibit slightly shorter axial M–O bond orders than the equatorial ones, which induces their compressed axial M–O distance. On the other hand, for the Pd^{2+} and Pt^{2+} ions, the bond orders of two orientations are larger than that of the third orientation, indicating the preference of Pd^{2+} and Pt^{2+} cations for square-planar coordination than for the octahedral sites.

3.6. The template effect of the hydrated metal ions in the construction of LDHs sheets related to the different types

The hexahydrated octahedral coordination cations, the initial template to form LDHs sheets, show different characters in different types. Therefore, whether an ion can combine with Mg^{2+} to form LDHs sheet easily is related closely to the type in which they are included, i.e., the distortion angles of their hexahydrated ions. From this point of view, we summarized the previous reports on different ions related to the formation of LDHs and made comparison with our calculations. Table S3 (Supplementary Information) lists the relationship between the reported ions which have been introduced into LDHs layers and the ionic classification in this work.

Table S3A indicates that the reported metal ions introduced into LDHs layers with relatively large amount (>10% atomic ratio percent) include more cations in Type I than in Type II, and the reported Type II ions are all in 3d transition period. When a hexahydrated cation in Type I combine with Mg^{2+} or Al^{3+}, the close distortion angles of them (the difference is not larger than 1.00°) would make each of them to be flatted with the similar angle to obtain a stable structure. As for 3d Type II ions, which have larger distortion angles than those of Type I, when combined with Mg^{2+} and Al^{3+}, the flatted angle of them will be different, which would need more energy to maintain a stable structure. This suggests that Type II ions are more difficult to be incorporate into the LDHs layer.

In spite of the fact that the 3d divalent ions in Type II can combine with Al^{3+} to construct binary LDHs layers, the resulting LDHs are usually not very stable to maintain pure phase, especially for Cu^{2+} ion owing to the relatively large distortion angle caused by strong Jahn–Teller effect [2]. Thus, they are generally to be incorporated into LDHs layers in the presence of other Type I or Type II cations with the same valence. For instance, Cu^{2+} ion could be introduced into the layers with a certain ratio of other divalent ions in order to get a stable layer structure. It has been reported that the atomic ratio of the divalent ions effects remarkably on the stability of the Cu-Ni-Mg-Al LDHs: a stable LDH can be obtained only under the condition of $Mg^{2+}/\sum(M^{2+}) = 0.250, Cu^{2+}/\sum(M^{2+}) < 0.438$ or $Mg^{2+}/\sum(M^{2+}) = 0.500, Cu^{2+}/\sum(M^{2+}) < 0.375$ [40]. Other cations such as Fe^{2+} and Co^{2+} which also show Jahn–Teller effect can be easily oxidized to trivalent cations. As a result, three-component LDHs containing one element with different valence such as Mg-Co(II)-Co(III) LDHs and Co-Fe(II)-Fe(III) LDHs have been reported by controlling preparation conditions [41,42]. The Ni^{2+} ion is the only divalent ion in Type II which can form stable binary LDHs with Type I ions for its weak Jahn–Teller effect (Table 2).

On the other hand, for the noble metals such as Ru^{3+}, Os^{3+}, Rh^{3+}, Ir^{3+} included in Type II and Pd^{2+} and Pt^{2+} ions (Table S3B) included in Type III, although there have been reports in an attempt to incorporate these ions into LDHs layers owing to their excellent catalytic properties, the resulting materials only contained trace amount of them (0.04–5.0% atomic ratio percent), or just be supported by LDHs, especially for Pt^{2+} and Pd^{2+} [8]. This is due to the stronger preference of Pd^{2+} and Pt^{2+}cations for square-planar coordination than the octahedral sites of brucite-type sheets of the LDHs structure. It has also been reported that Ru^{3+}, Rh^{3+} and Ir^{3+} can be introduced into the LDHs layers with trace amount but more easily than Pd^{2+} and Pt^{2+} [8h], which is in agreement with the distortion angles of their hexahydrated ions.

Based on the discussion above, it can be concluded that the easiness of the metal ions to be introduced into LDHs layers is in the following order: Type I > Type II > Type III. From this point of view, it is easy to understand the fact mentioned in the introduction section that both Pd^{2+} and Pt^{2+}, with much closer ionic radius to Mg^{2+}, were hard to be introduced into LDHs layer because of the large distortion angle (10.29° and 13.22°, respectively), which is related to their preferential coordination of fourfold but not the sixfold environment in a LDH layer.

In contrast, Ca^{2+} and Cd^{2+}, with much larger ionic radius than that of Mg^{2+}, have been reported to be incorporated into LDHs layers to form stable structure. Based on our calculation, although the octahedral sixfold hydrated ions are stable with small distortion angle (0.20° and 0.31°, respectively), their sevenfold coordination are more stable due to their large size. For Cd^{2+}, the coordination environment in Cd-Al-LDH is still unclear in report [10]. However, in fact, the reported Ca_2Al-LDHs are, indeed, among the most stable. And each Ca^{2+} in this structure can be more accurately described as being 7-coordinated, with the 7th oxygen being provided by a water molecule from the interlayer [9]. This is accordance with the calculation in this work, and also suggest that when an ion's size is much larger than that of Mg^{2+}, it is possible for it to get more than sixfold coordination with interlayer ions but not only coordinate with the oxygen in LDH layer, so as to obtain a more stable structure.

It should be pointed out that although Li^+ is classified into Type III in this work, many researchers reported its incorporation into LDHs layers (only Li-Al-LDHs) [6]. In fact, the formation mechanism of the well known unique Li-Al LDHs is different from that of the brucite-like M(II)-M(III) LDHs. The crystal structure of Li-Al LDH formulated by $[LiAl_2(OH)_6]^+[A^{n-}]_{1/n}{\cdot}yH_2O$ is derived from gibbsite (γ-$Al(OH)_3$) in which the lithium ions are located in the remaining one-third of the octahedral holes within the $Al(OH)_3$ layers which are not filled by Al^{3+} ions [6a]. From this point of view, it can also be understood that the Li^+ is an exception for the distortion angle rule in the construction of brucite-like LDHs based on our calculation.

Consequently, when the ion which is intend to be introduced into the LDHs layer has the close ionic radius to Mg^{2+}, the distortion angle of the octahedral hydrated ions plays a more important role to direct stability of the structure in the construction of LDHs layers. On the other hand, for the ions which have much larger size than Mg^{2+}, the possibility of their more-than-6 coordination preference is important in the formation of LDHs.

4. Conclusions

A series of density functional calculation of the hexahydrated octahedral coordination metal cations with model formula $[M(OH_2)_6]^{n+}$ (M = metal cation, n = 2, 3 and 1 for M = Li) were performed at DFT/B3LYP level, for the purpose of understanding the template effect of these ions in the formation of LDHs layers and finding out which cation can be introduced into the LDHs layers easily.

For the cation with similar ion size to Mg^{2+}, the computational models presented here have succeeded in exhibiting the structure directing relationship between initial template octahedral hexahydrated cations and the relative stability of related LDHs. The structural properties of the hexahydrated cations, such as metal–oxygen bond length, O–M–O bond angle distortion, binding energy, valence electronic configuration, ligand field, Jahn–Teller effect and natural bond orbital (NBO), which are related to the construction of LDHs layers have been systematically illustrated and were in good agreement with the experimental results.

In conclusion, the distortion angle of an octahedral coordination hexahydrated cation has been quantitatively revealed to play a significant role in the formation of LDHs layers on the basis of our DFT theoretical calculation results. The metal cations which can form the canonical hexahydrated structure with the distortion angle (θ) smaller than 1° are easily incorporated into LDHs layers to form stable structures, while those which form octahedral hexahydrated structure in heavy distortion with θ larger than 10° are difficult to be introduced into LDHs layers. Co-working with the ion size rule, the distortion angles of hexahydrated cations will surely play important part in giving clear hint to the design and preparation of LDHs and related materials with prospective applications.

Acknowledgements

This work was supported by the National Natural Science Foundation of China, the Program for New Century Excellent Talents in University (Project No.: NCET-05-121), the Program for Changjiang Scholars and Innovative Research Team in University (Grant No.: IRT0406) and the 111 Project (Grant No.: B07004).

Appendix A. Supplementary data

Total energies, zero-point corrected total energies and the frequency minima of the optimized $[Mg_n(OH_2)_{n+6}(OH)_{2n-2}]^{2+}$ (n = 2–7) clusters (Table S1) and $[M(OH_2)_6]^{n+}$ model structures (Table S2); comparison between the calculated ionic types and the experimental findings (Table S3); Cartesian coordinates of optimized models (Table S4). Supplementary information associated with this article can be found in the online version. Supplementary data associated with this article can be found, in the online version, at doi:10.1016/j.theochem.2008.06.031.

References

[1] (a) B.F. Sels, D.E. De Vos, P.A. Jacobs, Angew. Chem. Int. Ed. 44 (2005) 310;
(b) J.-H. Choy, S.-Y. Kwak, J.S. Park, Y.-J. Jeong, J. Portier, J. Am. Chem. Soc. 121 (1999) 1399;
(c) T. Itoh, T. Shichi, T. Yui, H. Takahashi, Y. Inui, K. Takagi, J. Phys. Chem. B 109 (2005) 3199;
(d) J.A. Gursky, S.D. Blough, C. Luna, C. Gomez, A.N. Luevano, E.A. Gardner, J. Am. Chem. Soc. 128 (2006) 8376;
(e) L. Mohanambe, S. Vasudevan, J. Phys. Chem. B 109 (2005) 15651;
(f) Z. Liu, R. Ma, M. Osada, N. Iyi, Y. Ebina, K. Takada, T. Sasaki, J. Am. Chem. Soc. 128 (2006) 4872;
(g) H. Chen, F. Zhang, S. Fu, X. Duan, Adv. Mater. 18 (2006) 3089;
(h) J.H. Lee, S. Rhee, D.-Y. Jung, J. Am. Chem. Soc. 129 (2007) 3522.

[2] (a) F. Cavani, F. Trifirò, A. Vaccari, Catal. Today 11 (1991) 173;
(b) V. Rives, M.A. Ulibarri, Coord. Chem. Rev. 181 (1999) 61;
(c) G.R. Williams, D. O'Hare, J. Mater. Chem. 16 (2006) 3065;
(d) A.I. Khan, D. O'Hare, J. Mater. Chem. 12 (2002) 3191.

[3] X. Duan, D.G. Evans (Eds.), Layered Double Hydroxides, Structure and Bonding, vol. 119, Springer, Berlin/Heidelberg, 2006, p. 3.

[4] S.P. Newman, H.C. Greenwell, P.V. Coveney, W. Jones, Layered Double Hydroxides: Present and Future, Nova Science, New York, 2001.

[5] (a) D. Tichit, S. Ribet, B. Coq, Eur. J. Inorg. Chem. (2001) 539;
(b) Z.P. Xu, H.C. Zeng, Chem. Mater. 13 (2001) 4555;
(c) V. Rives, A. Dubey, S. Kannan, Phys. Chem. Chem. Phys. 3 (2001) 4826;
(d) R.M. Rojas, D. Kovacheva, K. Petrov, Chem. Mater. 11 (1999) 3263;
(e) B. Mavis, M. Akinc, J. Power Sources 34 (2001) 308;
(f) S. Velu, K. Suzuki, S. Hashimoto, N. Satoh, F. Ohashi, S. Tomura, J. Mater. Chem. 11 (2001) 2049.

[6] (a) A.V. Besserguenev, A.M. Fogg, R.J. Francis, S.J. Price, D. O'Hare, V.P. Isupov, B.P. Tolochko, Chem. Mater. 9 (1997) 241;
(b) A.M. Fogg, J.S. Dunn, D. O'Hare, Chem. Mater. 10 (1998) 356;
(c) X. Hou, A.G. Kalinichev, R.J. Kirkpatrick, Chem. Mater. 14 (2002) 2078;
(d) A.M. Fogg, A.J. Freij, G.M. Parkinson, Chem. Mater. 14 (2002) 232.

[7] Note: the sixfold coordinated ionic radii in this paper are adopted from R.D. Shannon, Acta Crystallogr. A32 (1976) 751.

[8] (a) F. Basile, G. Fornasari, M. Gazzano, A. Vaccari, Appl. Clay Sci. 18 (2001) 51;
(b) S. Narayanan, K. Krishna, Appl. Catal. A Gen. 176 (1998) 221;
(c) Y. Chen, C. Liaw, L. Lee, Appl. Catal. A Gen. 177 (1999) 1;
(d) S. Narayanan, K. Krishna, Appl. Catal. A Gen. 198 (2000) 13;
(e) A. Morato, C. Alonso, F. Medina, Y. Cesteros, P. Salagre, J.E. Sueiras, D. Tichit, B. Coq, Appl. Catal. B Environ. 32 (2001) 167;
(f) S. Narayanan, K. Krishna, Catal. Today 49 (1999) 57;
(g) D. Tichit, O. Lorret, B. Coq, F. Prinetto, G. Ghiotti, Micropor. Mesopor. Mat. 80 (2005) 213;

(h) F. Basile, G. Fornasari, M. Gazzano, A. Vaccari, Appl. Clay Sci. 16 (2000) 185;
(i) H. Zhou, G. Zhuo, X. Jiang, J. Mol. Catal. A Chem. 248 (2006) 26.

[9] (a) A. Terzis, S. Filippakis, J. Kuzl, H. Burzhaff, Z. Kristallogr. 181 (1987) 29;
(b) B. Cherkashin, D. Reinter, Clay Clay Miner. 41 (1993) 631;
(c) G. Renaudin, M. Francois, Acta Cryst. C55 (1999) 835;
(d) M. Francois, G. Renaudin, O. Evard, Acta Cryst. C54 (1988) 1214.

[10] (a) F.M. Vivhi, O.L. Alves, J. Mater. Chem. 7 (1997) 1631;
(b) Y. Guo, H. Zhang, L. Zhao, G. Li, J. Chen, L. Xu, J. Solid State Chem. 178 (2005) 830.

[11] L.A. Estroff, A.D. Hamilton, Chem. Mater. 13 (2001) 3227.

[12] J. Li, J. Yu, W. Yan, Y. Xu, W. Xu, S. Qiu, R. Xu, Chem. Mater. 11 (1999) 2600.

[13] D.W. Britt, U.G. Hofmann, D. Mobius, S.W. Hell, Langmuir 17 (2001) 3757.

[14] (a) H.C. Greenwell, W. Jones, P.V. Coveney, S. Stackhouse, J. Mater. Chem. 16 (2006) 708;
(b) G.M. Lombardo, G.C. Pappalardo, F. Punzo, F. Costantino, U. Costantino, M. Sisani, Eur. J. Inorg. Chem. (2005) 5026;
(c) A.G. Kalinichev, R.J. Kirkpatrick, Chem. Mater. 14 (2002) 3539;
(d) H.C. Greenwell, W. Jones, S.P. Newman, P.V. Coveney, J. Mol. Struct. 647 (2003) 75;
(e) L. Mohanambe, S. Vasudevan, Langmuir 21 (2005) 10735;
(f) P.P. Kumar, A.G. Kalinichev, R.J. Kirkpatrick, J. Phys. Chem. B 110 (2006) 3841;
(g) S.P. Newman, S.J. Williams, P.V. Coveney, W. Jones, J. Phys. Chem. B 102 (1998) 6710;
(h) J.W. Wang, A.G. Kalinichev, R.J. Kirkpatrick, X. Hou, Chem. Mater. 13 (2001) 145;
(i) R.T. Cygan, J.J. Liang, A.G. Kalinichev, J. Phys. Chem. B 108 (2004) 1255;
(j) A.M. Aicken, I.S. Bell, P.V. Coveney, W. Jones, Adv. Mater. 9 (1997) 409;
(k) H. Li, J. Ma, D.G. Evans, T. Zhou, F. Li, X. Duan, Chem. Mater. 18 (2006) 4405.

[15] (a) J. Sauer, Chem. Rev. 89 (1989) 199;
(b) J. Sauer, P. Ugliengo, E. Garrone, V.R. Saunders, Chem. Rev. 94 (1994) 2095.

[16] (a) S. Stackhouse, P.V. Coveney, E. Sandre, J. Am. Chem. Soc. 123 (2001) 11764;
(b) H.C. Greenwell, S. Stackhouse, P.V. Coveney, W. Jones, J. Phys. Chem. B 107 (2003) 3476;
(c) K. Refson, S.-H. Park, G. Sposito, J. Phys. Chem. B 107 (2003) 13376;
(d) A. Trave, A. Selloni, A. Goursot, D. Tichit, J. Weber, J. Phys. Chem. B 106 (2002) 12291.

[17] L.G. Gorb, E.V. Aksenenko, J.W. Adams, S.W. Larson, C.A. Weiss, D. Leszczynska, J. Leszczynski, J. Mol. Struct. 425 (1998) 129.

[18] (a) R.C. Peterson, R.J. Hill, G.V. Gibbss, Can. Mineral. 17 (1979) 703;
(b) M. Pu, B. Zhang, Mater. Lett. 59 (2005) 3343;
(c) H. Sato, A. Morita, K. Ono, H. Nakano, N. Wakabayashi, A. Yamagishi, Langmuir 19 (2003) 7120;
(d) C.I. Sainz-Diaz, V. Timon, V. Botella, A. Hernandez-Laguna, Am. Mineral. 85 (2000) 1038.

[19] J.M. Ruiz, M.H. McAdon, J.M. Garces, J. Phys. Chem. B 101 (1997) 1733.

[20] (a) R. Àkesson, L.G.M. Pettersson, M. Sandstrom, U. Wahlgren, J. Am. Chem. Soc. 116 (1994) 8691;
(b) R. Àkesson, L.G.M. Pettersson, M. Sandstrom, P.E.M. Siegbahn, U. Wahlgren, J. Phys. Chem. 96 (1992) 10773;
(c) R. Àkesson, L.G.M. Pettersson, M. Sandstrom, U. Wahlgren, J. Am. Chem. Soc. 116 (1994) 8705.

[21] N.N. Greenwood, A. Earnshaw, Chemistry of Elements, Pergamon, Oxford, 1989.

[22] (a) A.D. Becke, Phys. Rev. A 38 (1988) 3098;
(b) C. Lee, W. Yang, R.G. Parr, Phys. Rev. B 37 (1988) 785;
(c) S.H. Vosko, L. Wilk, M. Nussair, Can. J. Phys. 58 (1980) 1200;
(d) A.D. Becke, J. Chem. Phys. 98 (1993) 5648.

[23] (a) P.J. Hay, W.R. Wadt, J. Chem. Phys. 82 (1985) 270;
(b) W.R. Wadt, P.J. Hay, J. Chem Phys 82 (1985) 284;
(c) P.J. Hay, W.R. Wadt, J. Chem. Phys. 82 (1985) 299.

[24] G.A. Petersson, M.A. Al-Laham, J. Chem. Phys. 94 (1991) 6081.

[25] (a) W. Stevens, H. Basch, J. Krauss, J. Chem. Phys. 81 (1984) 6026;
(b) W.J. Stevens, M. Krauss, H. Basch, P.G. Jasien, Can. J. Chem. 70 (1992) 612;
(c) T.R. Cundari, W.J. Stevens, J. Chem. Phys. 98 (1993) 5555.

[26] M.J. Frisch, G.W. Trucks, H.B. Schlegel, G.E. Scuseria, M.A. Robb, J.R. Cheeseman, J.A. Montgomery Jr., T. Vreven, K.N. Kudin, J.C. Burant, J.M. Millam, S.S. Iyengar, J. Tomasi, V. Barone, B. Mennucci, M. Cossi, G. Scalmani, N. Rega, G.A. Petersson, H. Nakatsuji, M. Hada, M. Ehara, K. Toyota, R. Fukuda, J. Hasegawa, M. Ishida, T. Nakajima, Y. Honda, O. Kitao, H. Nakai, M. Klene, X. Li, J.E. Knox, H.P. Hratchian, J.B. Cross, C. Adamo, J. Jaramillo, R. Gomperts, R.E. Stratmann, O. Yazyev, A.J. Austin, R. Cammi, C. Pomelli, J.W. Ochterski, P.Y. Ayala, K. Morokuma, G.A. Voth, P. Salvador, J.J. Dannenberg, V.G. Zakrzewski, S. Dapprich, A.D. Daniels, M.C. Strain, O. Farkas, D.K. Malick, A.D. Rabuck, K. Raghavachari, J.B. Foresman, J.V. Ortiz, Q. Cui, A.G. Baboul, S. Clifford, J. Cioslowski, B.B. Stefanov, G. Liu, A. Liashenko, P. Piskorz, I. Komaromi, R.L. Martin, D.J. Fox, T. Keith, M.A. Al-Laham, C.Y Peng, A. Nanayakkara, M. Challacombe, P.M.W. Gill, B. Johnson, W. Chen, M.W. Wong, C. Gonzalez, J.A. Pople, Gaussian 03, Revision B.04, Gaussian, Inc., Pittsburgh, PA, 2003.

[27] (a) A.E. Reed, L.A. Curtiss, F. Weinhold, Chem. Rev. 88 (1988) 899;
(b) J.P. Foster, F. Weinhold, J. Am. Chem. Soc. 102 (1980) 7211.

[28] (a) E.D. Glendening, A.E. Reed, J.E. Carpenter, F. Weinholk, NBO, version 3.1;
(b) E.D. Glendening, J.K. Badenhoop, A.E. Reed, J.E. Carpenter, J.A. Bohmann, C.M. Morales, F. Weinhold, NBO, version 5.0.

[29] M. Wendt, F. Weinhold, NBOView, version 1.1.

[30] (a) F. Zigan, R. Rothbauer, Neues. Jahrb. Mineral. Monatsh. 4–5 (1967) 245;
(b) P. Baranek, A. Lichanot, R. Orlando, R. Dovesi, Chem. Phys. Lett. 340 (2001) 362.

[31] (a) E.S. Marcos, R.R. Pappalardo, J. Phys. Chem. 95 (1991) 8928;
(b) W.R. Busing, H.A. Levy, J. Chem. Phys. 26 (1957) 563;
(c) E.N. Maslen, S.C. Ridout, K.J. Watson, Acta Crystallogr. B 44 (1988) 96;
(d) A.K. Katz, J.P. Glusker, S.A. Beebe, C.W. Bock, J. Am. Chem. Soc. 118 (1996) 5752;
(e) M. Seth, M. Dolg, P. Fulde, P. Schwerdtfege, J. Am. Chem. Soc. 117 (1995) 6597.

[32] (a) B.J. Mhin, S. Lee, S.J. Cho, K. Lee, K.S. Kim, Chem. Phys. Lett. 197 (1992) 77;
(b) S. Lee, J. Kim, J.K. Park, K.S. Kim, J. Phys. Chem. 100 (1996) 14329;
(c) H.S. Choi, S.B. Suh, S.J. Cho, K.S. Kim, Proc. Natl. Acad. Sci. USA 95 (1998) 12094;
(d) C.W. Bock, A. Kaufman, J.P. Glusker, Inorg. Chem. 33 (1994) 419427;
(e) H. Erras-Hanauer, T. Clark, R. van Eldik, Coord. Chem. Rev. 238–239 (2003) 233;
(f) G.N. Merrill, S.P. Webb, D.B. Bivin, J. Phys. Chem. A 107 (2003) 386;
(g) C.W. Bock, A.K. Katz, J.P. Glusker, J. Am. Chem. Soc. 117 (1995) 3754;
(h) F.P. Rotzinger, J. Phys. Chem. B 109 (2005) 1510.

[33] (a) A. Veerman, H.M. Lee, K.S. Kim, J. Chem. Phys. 123 (2005) 084321;
(b) H.M. Lee, P. Tarakeshwar, J. Park, M.R. Kołaski, Y.J. Yoon, H.-B. Yi, W.Y. Kim, K.S. Kim, J. Phys. Chem. A 108 (2004) 2949;
(c) N.J. Singh, A.C. Olleta, A. Kumar, M. Park, H.-B. Yi, I. Bandyopadhyay, H.M. Lee, P. Tarakeshwar, K.S. Kim, Theor. Chem. Acc. 115 (2006) 127.

[34] B. Kallies, R. Meier, Inorg. Chem. 40 (2001) 3101.

[35] H.L. Schläfer, G. Gliemann, Basic Principles of Ligand Field Theory, John Wiley & Sons Ltd., 1969.

[36] H. Ohtaki, T. Radnai, Chem. Rev. 93 (1993) 1157.

[37] (a) N.A. Hewish, G.W. Neilson, J.E. Enderby, Nature 297 (1982) 138;
(b) F.M. Floris, M. Persico, A. Tani, J. Tomasi, Chem. Phys. Lett. 227 (1994) 126.

[38] G. Frenking, N. Fröhlich, Chem. Rev. 100 (2000) 717.

[39] S.J. Wilkens, W.M. Westler, J.L. Markley, F. Weinhold, J. Am. Chem. Soc. 123 (2001) 12026.

[40] Y. Feng, D. Li, C. Li, Z. Wang, D.G. Evans, X. Duan, Clay Clay Miner. 51 (2003) 566.

[41] (a) Z. Xu, H. Zeng, J. Mater. Chem. 8 (1998) 2499;
(b) J.T. Sampanthar, H. Zeng, Chem. Mater. 13 (2001) 4722.

[42] J. Liu, F. Li, D.G. Evans, X. Duan, Chem. Commun. (2003) 542.